SYNTHESIS OF MESOPOROUS TITANIA BY HOMOGENEOUS HYDROLYSIS OF TITANIA OXO-SULFATE IN THE PRESENCE OF CATIONIC AND ANIONIC SURFACTANTS

VÁCLAV ŠTENGL, VENDULA HOUŠKOVÁ[#], NATALIYA MURAFA, SNEJANA BAKARDJIEVA

Institute of Inorganic Chemistry AS CR v.v.i., 250 68 Řež, Czech Republic

[#]Corresponding author, e-mail: houskova@iic.cas.cz

Submitted January 20, 2010; accepted July 1, 2010

Keywords: Surfactant, Titania, Mesoporous, Photocatalyst

Mesoporous titania was prepared by homogeneous hydrolysis of titanium oxo-sulphate with urea in aqueous solutions in the presence of the cationic and anionic surfactants, cetyl trimethyl ammonium bromide (CTAB) and sodium dodecyl benzene sulfonate (SDBS), respectively. Following annealing at 600°C the structure of prepared samples was determined with X-ray powder diffraction (XRD) and selected area electron diffraction (SAED). The morphology and microstructure characteristics were also obtained by scanning electron microscopy (SEM) and high resolution electron microscopy (HRTEM). Surface area (BET) and porosity were also determined. The prepared mesoporous titania samples showed considerably higher photocatalytic activity compared to reference samples prepared without surfactants and with P25 Degussa.

INTRODUCTION

Mesoporous titania has attracted much attention since its high surface-to-volume ratio offers potentially more active reaction sites, making it of great importance in, for example, photocatalysis and photoelectrical chemical conversion. Therefore, worldwide research activity on mesoporous TiO_2 has followed.

The effectiveness of titania in practical photocatalytical applications many structural parameters are important such as particle size, surface area and porosity composition, crystallinity and, importantly, the morphology and texture of the titania material.

Controlled synthesis allows to prepare TiO_2 with very different morphology and structural architectures, such as single crystals, films, foams, nanotubes, nanowires, nanorods, nanowhiskers, porous networks, spherical particles and mesoporous titania.

High photocatalytic activity of mesoporous titania can not be explained solely on the basis of the size of surface surface. Such higher than expected photocatalytic activity may be explained by the presence of interior channels in the mesoporous photocatalysts. These channels may exhibit two beneficial effects on titania, namely, increasing the efficiency of photo-absorption and improving mass transfer. The overall photocatalytic activity is governed by three properties: photo-absorption efficiency, efficiency of the reaction of photo-generated electron/hole, and their combination, the first of which is strongly influenced by the mesoporous structure of titania. In the mesoporous stucture of titania photocatalyst, the channels acted as a light-transfer path for introducing incident photon flux onto the inner surface of mesoporous titania. This allowed light waves to penetrate deep inside the titania, making it a more efficient light harvester. Considering the light absorption, reflection, and scattering within such a mesoporous system, the effective light-activated surface area can be significantly enhanced.

To prepare mesoporous titania was already published many different syntheses. Industrial $TiOSO_4$ solution was used as an inorganic precursor to prepare mesoporous titania via a composite template route, using tri-block copolymer $EO_{20}PO_{70}EO_{20}$ (P-123) [1], using cetyl trimethyl ammonium bromide (CTAB) [2-7] or sodium dodecyl sulfate [8-12] as surfactant-directing agent and pore-forming agent. Nanocrystalline mesoporous titania was synthesized by sol-gel metod [13, 14], via a combined sol-gel process with surfactant-assisted templating method [15], by urea-templated sol-gel reactions [16] and by latex templates [17]. The sonochemical method has been developed to synthesize mesoporous TiO_2 nanorods using industrial bulk Ti powder [18] and by sonochemical synthesis of mesoporous chiral titania using a chiral inorganic precursor [19].

Nanocrystalline mesoporous titania was synthesized by hydrothermal method using titanium butoxide as starting material [20], tetrabutyl titanate [21], complex titanyl oxalate acid $H_2TiO(C_2O_4)_2$ [22] and from industrial titanyl sulfate solution under ultrasonic irradiation, microwave and hydrothermal condition [23]. In the present work, the role played by the interactions between the simple cationic (CTAB) and anionic surfactant (SDBS) respectively and the TiO_2 surface during homogeneous hydrolysis growth step are investigated. The relative photocatalytic activities of the prepared samples were assessed by the photocatalytic decomposition of Orange 2 dye.

EXPERIMENTAL

Preparation of mesoporous titania samples

All chemical reagents used in the present experiments were obtained from commercial sources and used without further purification. $TiOSO_4$, CTAB, SDBS and urea were supplied by Fluka, Munich, Germany.

The mesoporous titania was prepared by homogeneous hydrolysis of $TiOSO_4$ aqueous solutions in the presence of CTAB and SDBS, respectively. Urea was used as the precipitation agent. In a typical preparation, 100g $TiOSO_4$ was dissolved in 100 mL hot distilled water acidified with 98% H_2SO_4 (to pH ~ 1.2). The transparent liquid was diluted into 4 L of distilled water, a defined amount of CTAB or SDBS added (see Table 1) and mixed with 300 g of urea. The mixture was heated to 100°C under stirring and kept at this temperature for 9 h until pH 7.5 was reached and ammonia escaped from the solution. The formed precipitates were washed by distilled water with decantation, filtered and dried at temperature of 105°C in a drying oven. Using this method six samples were prepared. In the remainder of this paper, they will be denoted as TiCTAB_1 - TiCTAB_6 and TiDCB_1 - TiDCB_6, respectively. The reference sample (Ti_300) was prepared without surfactant. In order to remove residual surfactants the prepared samples were heated to 600°C for one hour under dynamic vacuum, using a quartz tube furnace controlled by the PID controller. The temperature increase rate was 1 °C/min. After the heat treatment, the sample was allowed to cool to room temperature.

Characterization methods

The surface area of samples out-gassed for 60 min at 150°C was determined from nitrogen adsorption-desorption isotherms at liquid nitrogen temperature using a Quantachrom Nova2000 instrument. The Langmuir-B.E.T. method was used for surface area calculation [24], while pore size distribution (pore diameter and volume) was determined by the B.J.H. method [25].

Transmission electron microscopy (TEM and HRTEM) micrographs were obtained by using two instruments, namely a Philips EM 201 at 80 kV and a JEOL JEM 3010 at 300 kV (LaB_6 cathode). A copper grid coated with an amorphous perforated carbon film was used to prepare samples for the TEM observation. A powdered sample was dispersed in ethanol and the suspension was treated in an ultrasonic bath for 10 minutes prior to analysis.

Scanning electron microscopy (SEM) studies were performed using a Philips XL30 CP microscope equipped with EDX (energy dispersive X-ray), Robinson, SE (secondary electron) and BSE (back-scattered electron) detectors. The sample was placed on an adhesive C slice and coated with a layer of Au-Pd alloy (10 nm thick).

Table 1. Experimental conditions, BET and pore size distribution of prepared samples.

Sample	CTAB/SDBS (g)	Crystallite size (nm)	Surface area (m^2/g)	Pore radius (Å)	Pore volume (cm^3/g)
TIT300	-	30.2	62.1	27.7	0.099
TiCTAB_1	1.0	19.2	65.9	32.7	0.122
TiCTAB_2	5.0	18.5	97.3	32.9	0.200
TiCTAB_3	7.5	18.3	69.8	39.0	0.256
TiCTAB_4	10.0	16.1	79.9	33.3	0.152
TiCTAB_5	12.5	13.2	99.9	39.5	0.211
TiCTAB_6	15.0	10.8	95.6	47.1	0.223
TiDCB_1	1.0	16.3	77.4	39.4	0.140
TiIDCB_2	5.0	16.0	86.4	39.6	0.222
TiDCB_3	7.5	15.2	78.4	32.1	0.198
TiDCB_4	10.0	13.7	72.4	24.9	0.127
TiDCB_5	12.5	13.0	114.1	48.8	0.233
TiDCB_6	15.0	13.3	105.8	48.6	0.246

X-ray diffraction (XRD) patterns were obtained using a Siemens D5005 instrument (Cu-Kα radiation (40 kV, 30 mA); diffracted beam monochromator). Qualitative analysis was performed with the Eva Application and the Xpert HighScore using the JCPDS PDF-2 database [26]. The crystallite size of the samples was calculated from the Scherrer equation [27] using the X-ray diffraction peak at 2Θ = 25.4° (anatase).

The photocatalytic activity of samples was assessed from the kinetics of the photocatalytic degradation of 0.02 M Orange 2 dye (sodium salt 4-[(2-hydroxy-1-naphtenyl)azo]-benzenesulfonic acid) in aqueous slurries. The azo-dyes (Orange 2, Methyl Red, Congo Red etc.) are not absorbed on titania surfaces in contrast to methylene blue. For azo-dye degradation, the complete mass balance in nitrogen indicated that the central –N=N– azo-group was converted in gaseous dinitrogen, which is ideal for the elimination of nitrogen-containing pollutants, not only for environmental photocatalysis but also for any physicochemical method [28]. The kinetics of the photocatalytic degradation of aqueous Orange 2 dye solution was measured using a self-constructed photoreactor [29, 30]. The photoreactor consists of a stainless steel cover and quartz tube with florescent lamp (254 nm and 365 nm) with a power of 13W and light intensity of 3.5mW/cm^2. The Orange 2 dye solution was circulated by a membrane pump through a flow cuvette. The concentration of Orange 2 dye was determined by the measurement of absorbance at 480 nm with a VIS spectrophotometer ColorQuestXE.

RESULTS AND DISCUSSION

It is well known that homogeneous hydrolysis of metal salts with urea leads to spherical crystalline nanoparticles of corresponding metal oxides [31, 32]. For example, by hydrolysis of $TiOSO_4$ with urea stable spherical, 1-2 μm in size, TiO_2 microporous particles are formed [33]. For these solids, minimisation of the surface energy leads to sphericity (see Figure 4a and 5a). The final particle shape depends on whether oriented or isotropic aggregation takes place. Among the various factors that control the aggregation, dispersive forces and electrostatic inter-particle interactions are the most important. Oriented aggregation is a consequence of the dissimilar electrostatic charges that develop on the different crystal faces of the primary particles, which aggregate in the directions of minimum repulsion; this phenomenon occurs mainly when the overall particle charge is large. On the other hand, isotropic aggregation, which usually leads to the formation of spherical particles, takes place in the vicinity of the isoelectric point. The presence of the surfactants changed the surface energy and prevented formation of the spherical particles.

X-Ray Diffraction (XRD)

In all the XRD patterns of precipitated samples, no peak was observed in the low angle range (2θ = 1–10°). This suggests the absence of an ordered mesoporous network structure in the as prepared samples. The as-

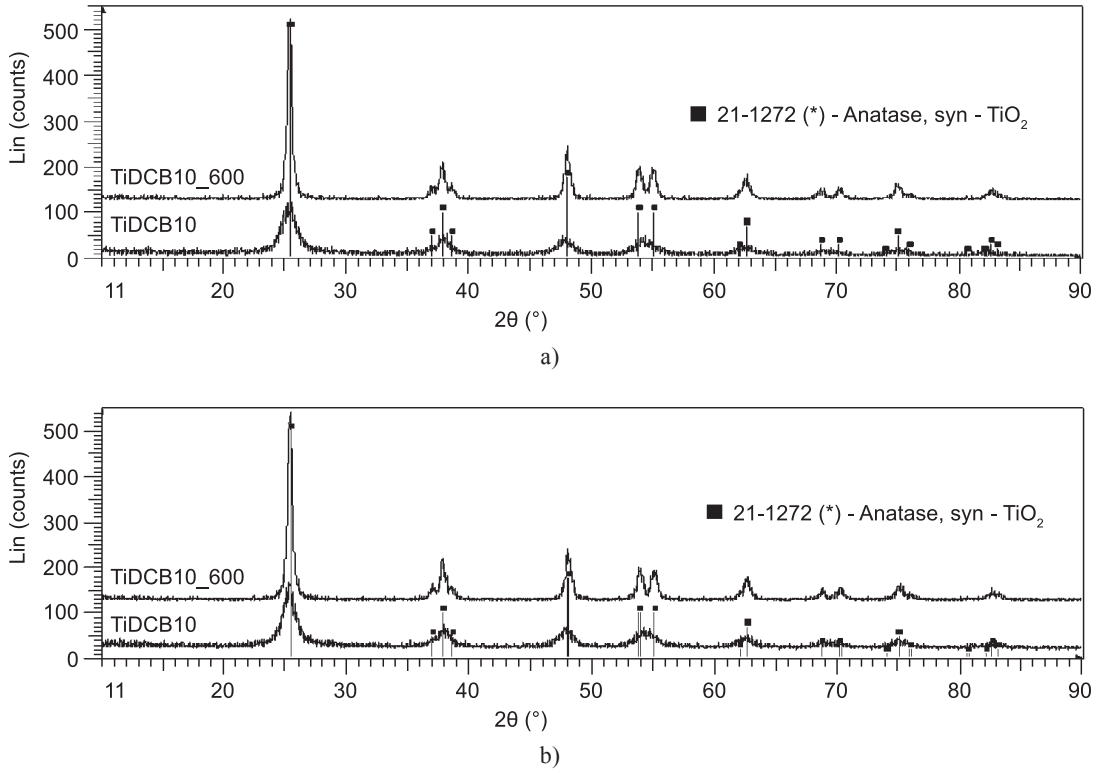

Figure 1. XRD pattern of the samples before and after annealing at 600°C; a) sample TiCTAB_4; b) sample TiDCB_4.

synthesized TiO_2 powders show broad anatase peaks (see Figure 1), indicating that the as-synthesized samples are anatase phase (JCPDS 21-1272). The Scherrer [19] line width analysis of the (1 0 1) reflection gives an estimate of the primary crystallite size in the range of 4-5 nm. After heat treatment, only peaks of the anatase phase that become stronger and sharper are identified in all prepared samples (see Figure 1). Average crystalline sizes calculated from the broadening of the (101) XRD peaks of the anatase phase are presented in Table 1 for the samples calcined at temperature 600°C. The crystalline size decreased with increased amount of surfactants. Usage of surfactants, which are able to change surface properties of reagents and therefore change microstructure of final products, results in particle sizes reduction.

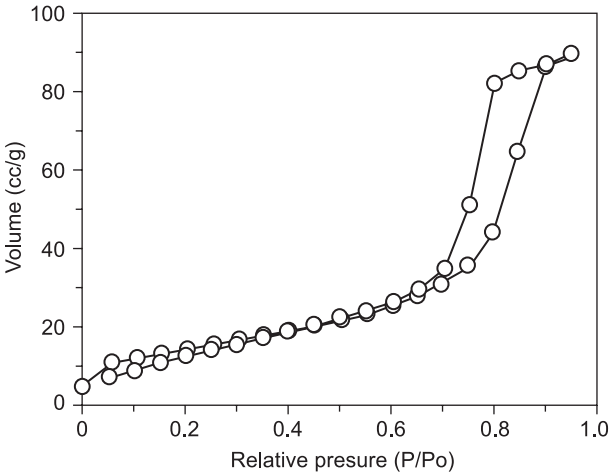

Figure 2. Nitrogen adsorption–desorption isotherms of the sample TiCTAB_4.

Surface area and porosity

Nitrogen adsorption-desorption isotherms and BJH pore size distribution plots of desorption d$V(r)$ versus pore radius and d$S(r)$ versus pore radius of selected samples are shown in Figures 2 and 3. These type IV isotherms with a hysteresis loop are typical of mesoporous materials [34]. The pore size distribution (see

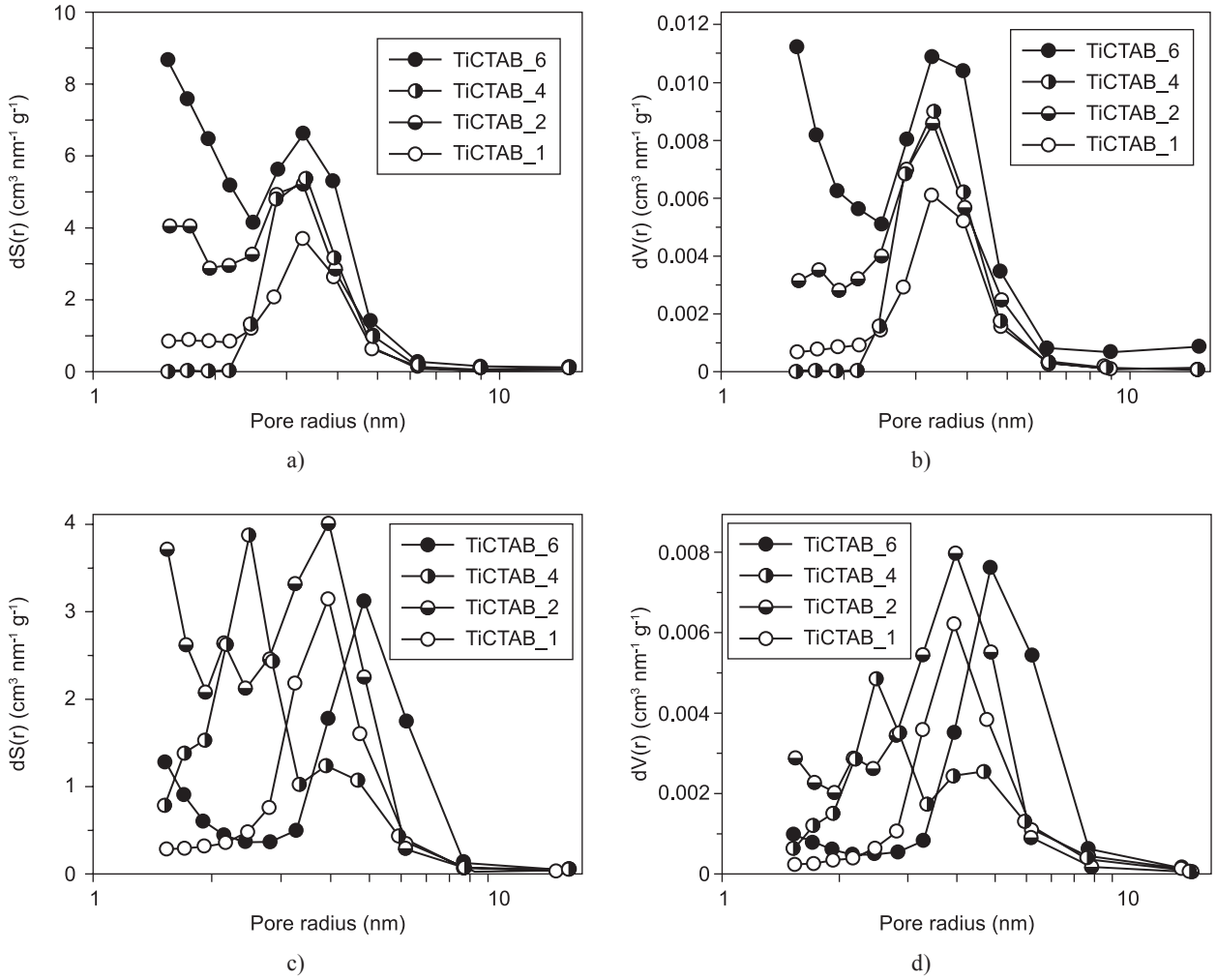

Figure 3. BJH pore size distribution plots of a) desorption d$S(r)$ of the samples TiCTAB, b) d$V(r)$ of the samples TiCTAB, c) desorption d$S(r)$ of the samples TiDCB, d) d$V(r)$ of the samples TiDCB versus pore radius.

Figure 3) of the as-synthesised samples determined by BJH desorption isotherm shows a bimodal pore size distribution consisting of smaller fine (~ 2 nm) with intra-particle pores and larger (~ 5 nm) inter-particle pores. The pore structural parameters of all samples are listed in Table 1. Compared to the reference sample prepared without surfactants (denoted as TIT300), the surface area, pore volume and pore radius increases with the amount of surfactant presented during the preparation. This effect cohere with that in previous chapter, namely with decreasing of crystalline size of samples. Amount of anionic surfactant SDBS has limiting value (12.5 g), to which is specific surface area, pore volume and pore radius decreased. This can be affected by reaching of critical micelle concentration (CMC). In chemistry, the critical micelle concentration (CMC) is defined as the concentration of surfactants above which micelles are spontaneously formed. According to the literature, the CMC value of CTAB is in range of 0.9-1.0 mM and the CMC value of SDBS is in range of 1.2-1.6 mM.

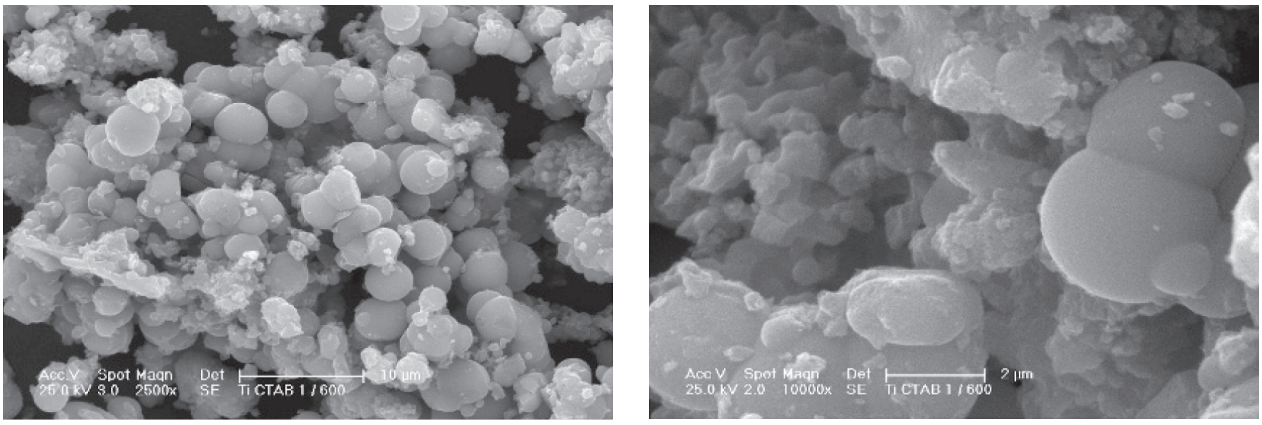

a)

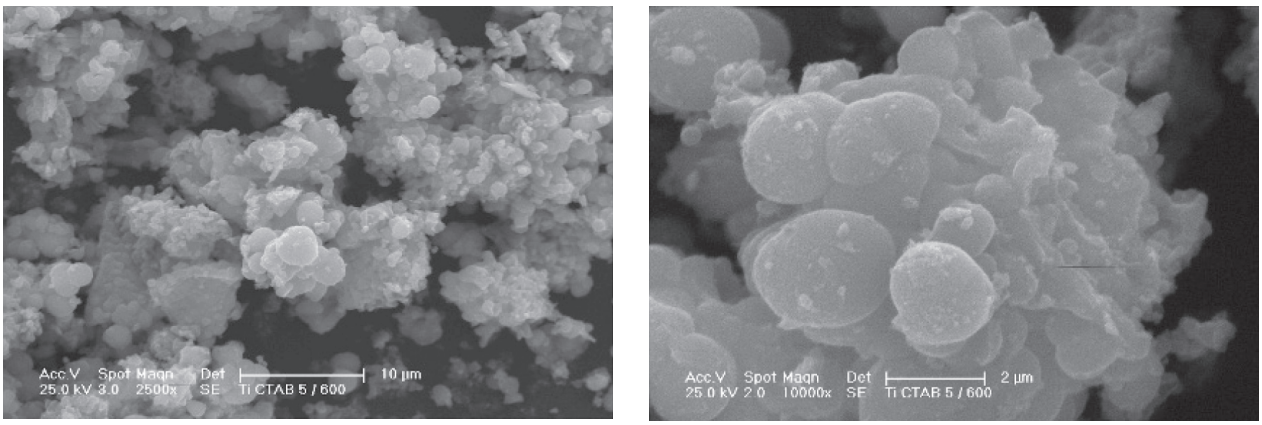

b)

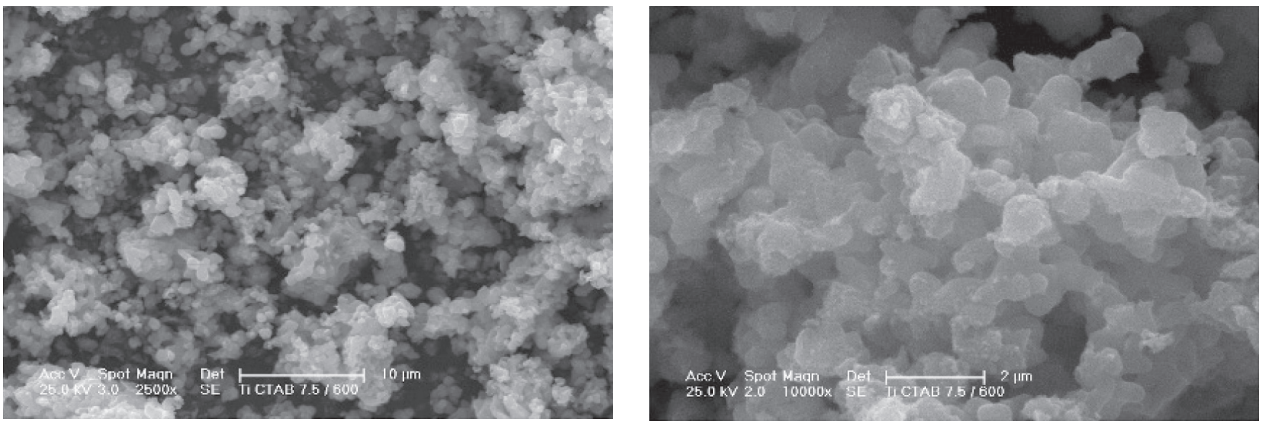

c)

Figure 4. SEM micrographs of samples a) TiCTAB_1, b) TiCTAB_2, c) TiCTAB_3.

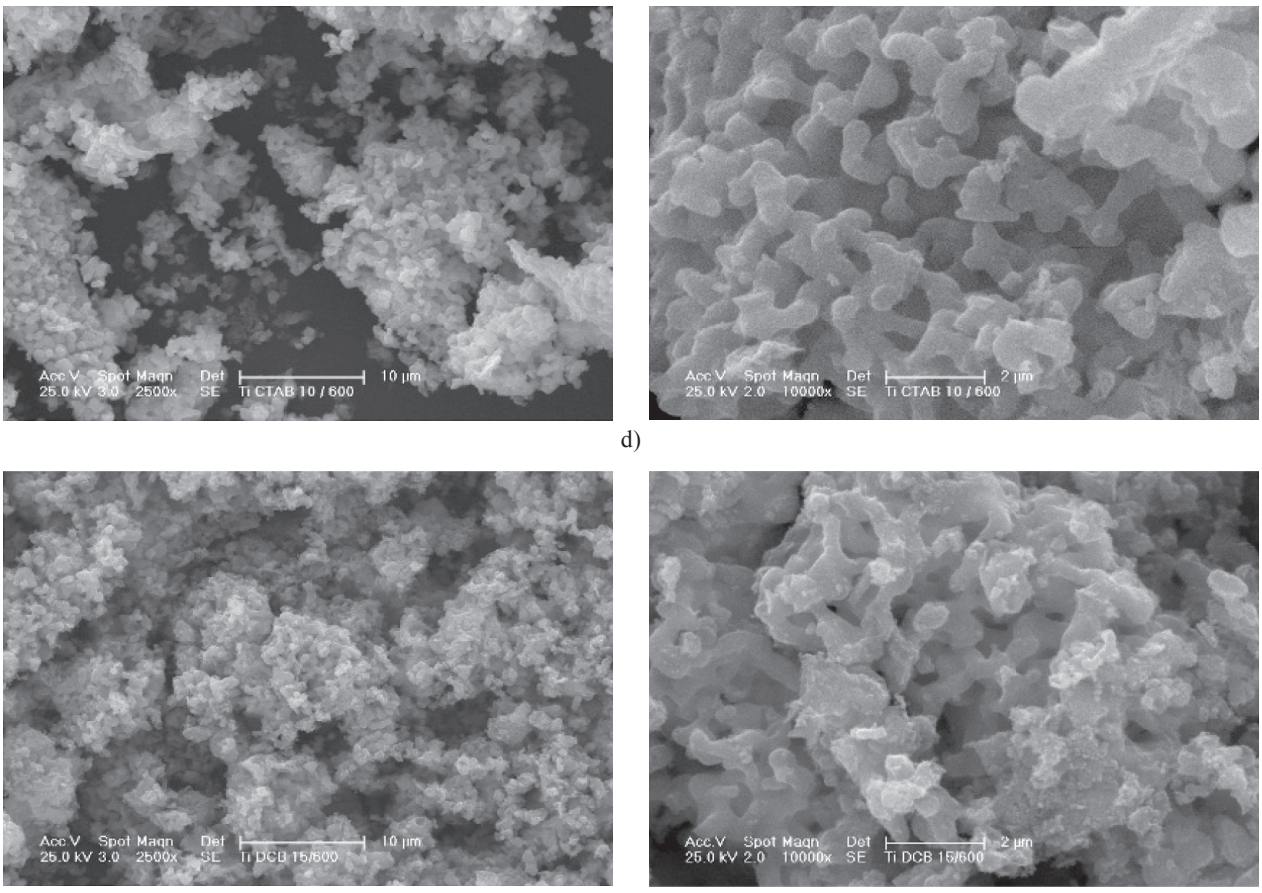

Figure 4. SEM micrographs of samples d) TiCTAB_4, e) TiCTAB_6; enlarged in the right side of picture.

Scanning electron microscopy (SEM) and Transmission electron microscopy (HRTEM)

The SEM images of the prepared samples are presented in Figures 4 and 5. The SEM micrographs show roughly spherical particles that are ~2 µm in size, when 1g of CTAB and SDBS respectively, were used (see Figure 4a and 5a). When the concentration of the surfactants in the reaction mixture is increased, the spherical particles are transformed to the mesoporous phase (coral-like structures, see Figures 4d and 5d). The three structures are formed on the surface of TiO_2 in the order of increasing CTAB and SDBS concentration respectively, have been attributed to the creation of hemimicelle, admicelle, and micelle structures (see Figure 6) on the surface [35]. A hemimicelle is described as a patchy bilayer in which the second layer is incomplete. The admicelle can be described as a more complete or less defective bilayer structure. At the highest CTAB concentration (1 mM), true micelles adsorb on the surface.

Results obtained by high resolution transmission electron microscopy (HRTEM) and electron diffraction (ED) are shown in Figures 7 and 8. The micellar structures created on the TiO_2 surface in the unheated sample named TiCTAB_4 is presented in Figure 7a and b (arrow). Figure 7b shows that the micelles form a worm-hole-like pore texture and that the diameter of these wormhole-like pores is distributed in the range of 2-3 nm. The HRTEM micrographs in Figure 8 characterised the surface morphology of the sample heated at 600°C (TiCTAB_4) and show that the heated sample has an interlayer spacing of 0.352 nm corresponding to the (101) plane of anatase (see Figure 8c). According to HRTEM results the mesoporous TiO_2 consist of primary nanocrystals with perfect crystal structure. The selected area of diffraction patterns (see Figure 8c) confirmed the anatase phase.

Photocatalytic activity

The photocatalytic activity of the prepared samples was determined using the degradation of 0.02 M Orange 2 dye aqueous solutions under UV radiation at 254 nm (UV-C, germicidal white lamp) and 365 nm (UV-A, fluorescent black lamps). In regions in which the Lambert-Beer law is valid, the concentration of the Orange 2 dye is proportional to absorbance:

$$A = \varepsilon\, c\, l \qquad (1)$$

where A is absorbance, c is concentration of absorbing component, l is length of absorbing layer and ε is molar absorbing coefficient. The time dependence of Orange 2

dye decomposition can be described using Equation (2) for a reaction following first-order kinetics [36]:

$$\frac{d[OII]}{dt} = k(a_0 - [OII]) \quad (2)$$

where [OII] is the concentration of Orange 2 dye, a_0 is the initial concentration of Orange 2 dye and k is the rate constant. It is easily seen in Figure 9, that the first order kinetics curves (plotted as lines) fitted all the experimental points. For comparison, the photocatalytic activity of a commercially available photocatalyst (Degussa P25) and anatase prepared without surfactant were also tested. The calculated degradation rate constants k are listed in Table 2 and the kinetic degradation of Orange 2 dye at 254 nm and 365 nm wavelength of the samples TiCTAB_4, TiDCB_4, TIT300 (reference sample prepared without surfactant and heated at 600°C) and Degussa P25 respectively, are presented in Figure 9. Clearly, the highest photocatalytic activities are shown by TiCTAB_4 and TiDCB_5, prepared with 10g of

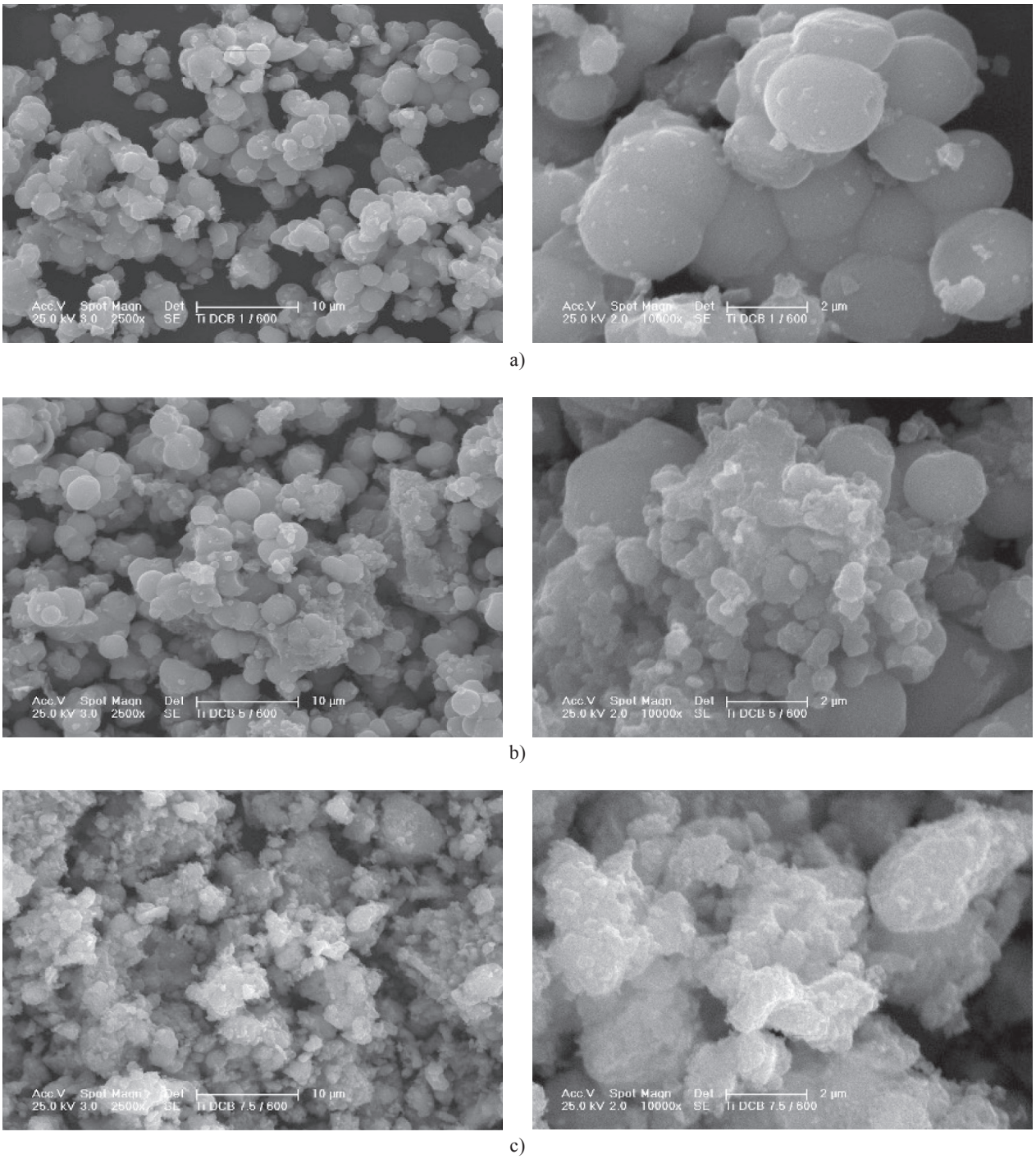

Figure 5. SEM micrographs of samples a) TiDCB_1, b) TiDCB_2, c) TiDCB_3; enlarged in the right side of picture.

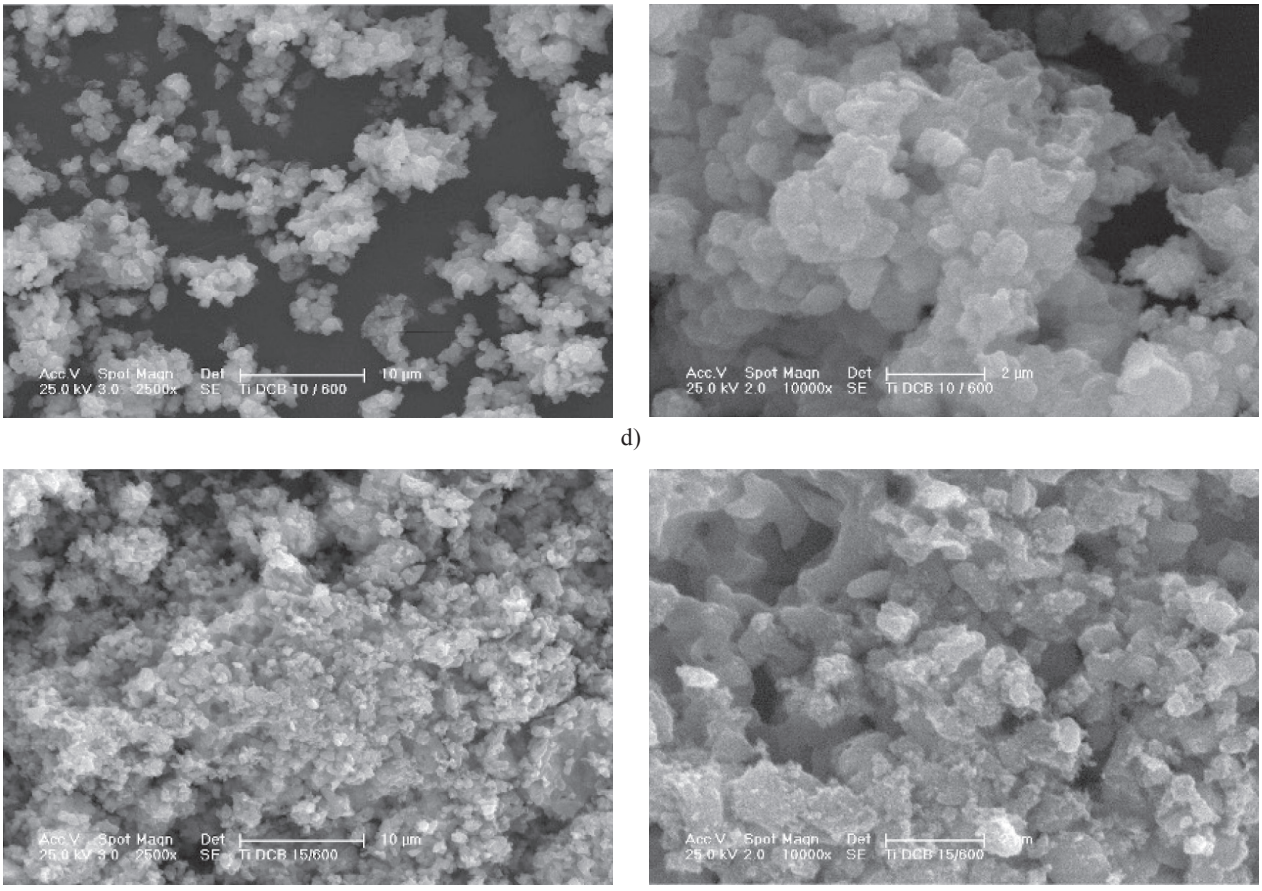

Figure 5. SEM micrographs of samples d) TiDCB_4, e) TiDCB_6; enlarged in the right side of picture.

CTAB and 12.5 g SDBS, respectively. These samples are prepared with higher content of surfactants, which effect particle shape changes, crystallite size decreasing and growth of specific surface area. To the contrary, too high content of surfactants causes occurrence of amorphous domains (confirmed by HRTEM) and therefore causes decreasing of photocatalytic activity.

Table 2. Photocatalytic constant k for the photodegradation of Orange 2 (λ = 254, 365 nm).

Sample	*k* at 254 nm (min^{-1})	*k* at 365 nm (min^{-1})
TiCTAB_1	0.2358	0.0631
TiCTAB_2	0.2544	0.0901
TiCTAB_3	0.2521	0.1155
TiCTAB_4	0.3974	0.1556
TiCTAB_5	0.1725	0.0641
TiCTAB_6	0.1453	0.0572
TiDCB_1	0.1455	0.0333
TiDCB_2	0.1736	0.0403
TiDCB_3	0.2597	0.0501
TiDCB_4	0.3072	0.1762
TiDCB_5	0.4906	0.2080
TiDCB_6	0.1647	0.0605
TIT300	0.2260	0.0695
P 25	0.1907	0.0987

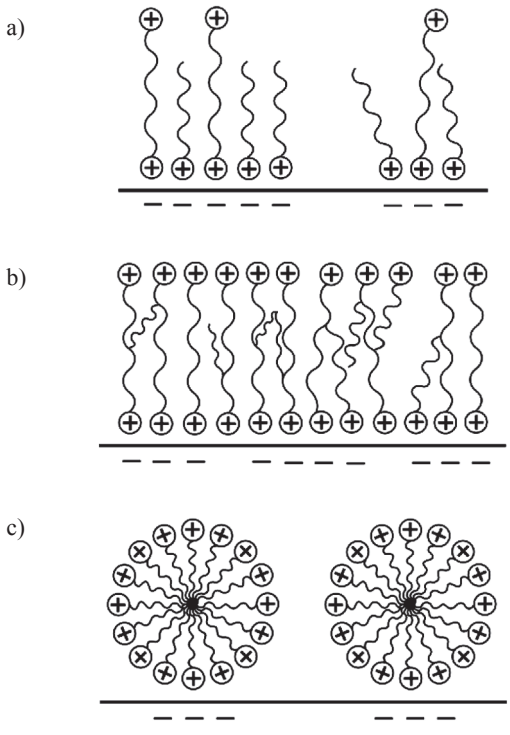

Figure 6. Structures formed with CTAB and SDBS, a) hemimicellar, b) admicellar, and c) micellar.

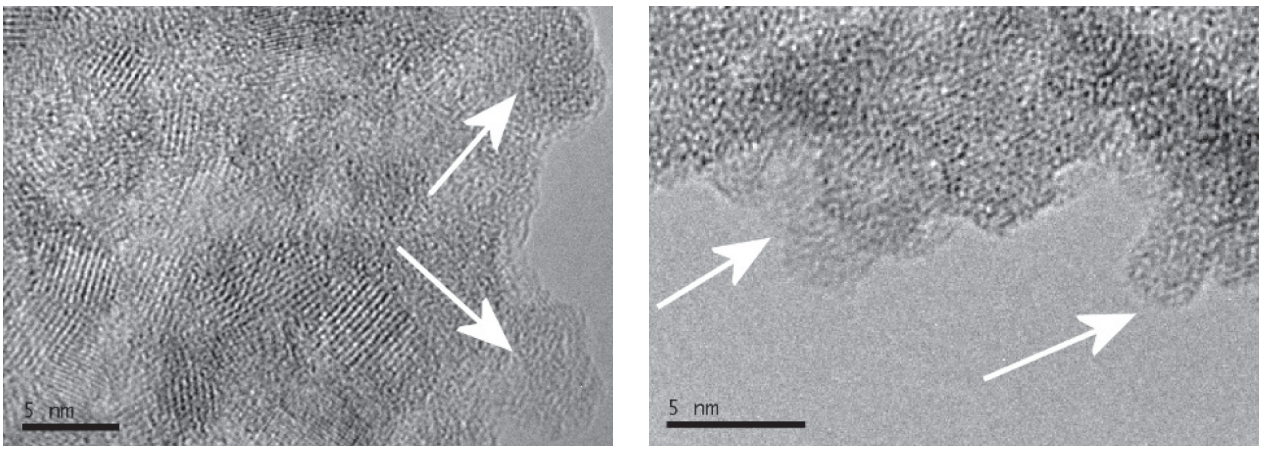

a) b)

Figure 7. HRTEM micrograph of unheated sample TiCTAB_4; a) micellar structure, b) wormhole-like structure.

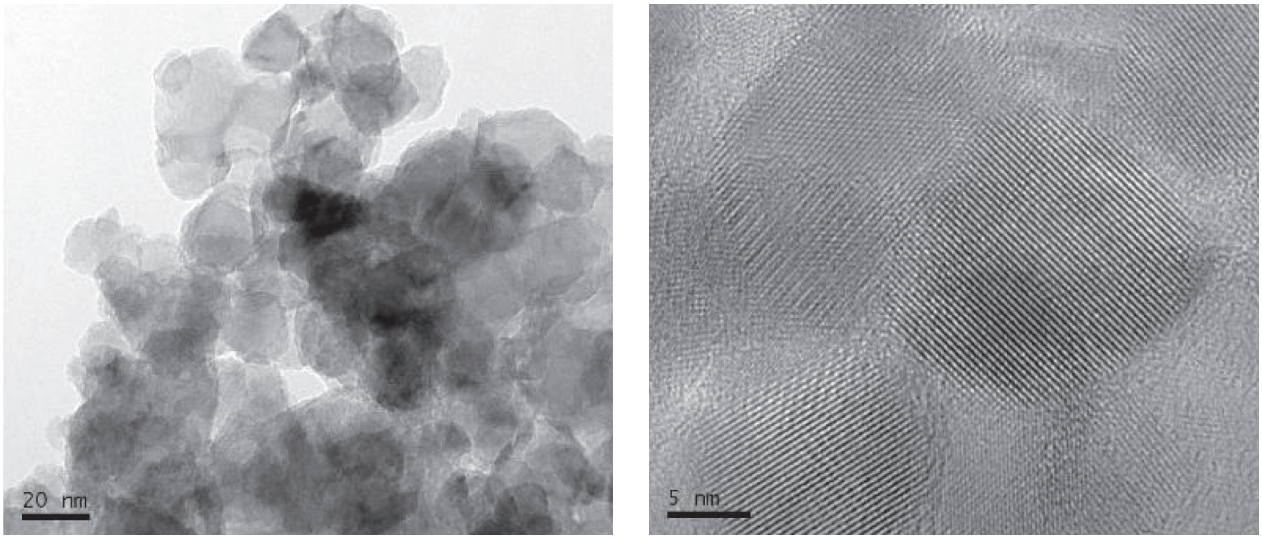

a) b)

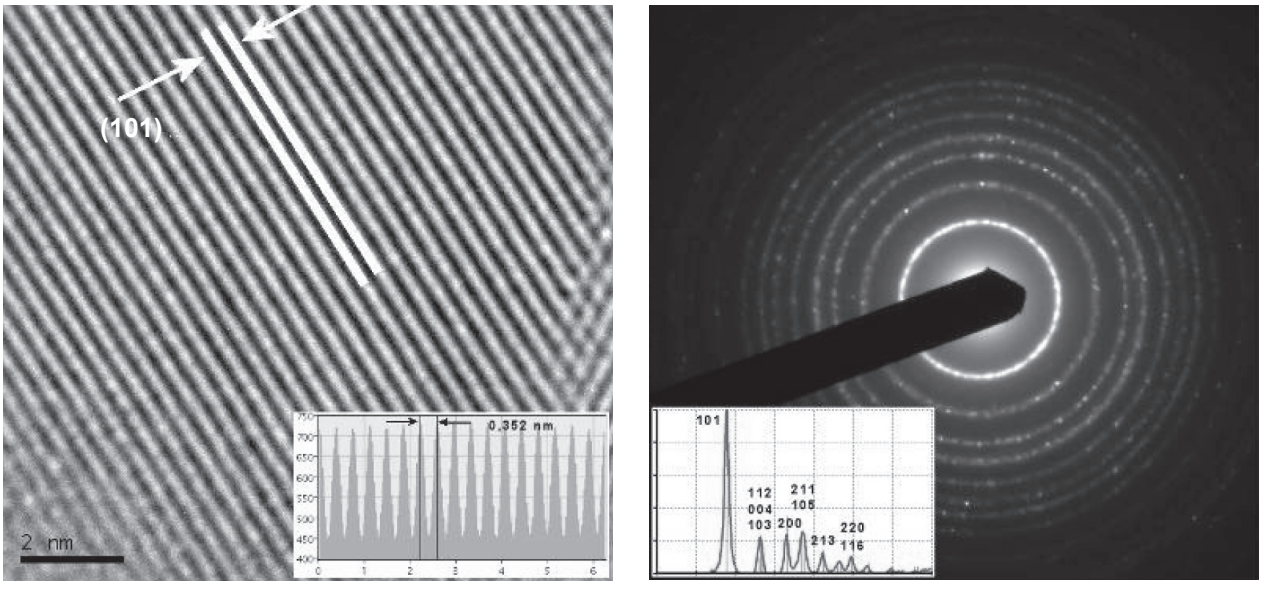

c) d)

Figure 8. HRTEM micrograph of sample denoted as TiCTAB_4 heated at 600°C; a) magnification 100 000x, b) magnification 500 000x, c) magnification 1 500 000x, d) SAED pattern.

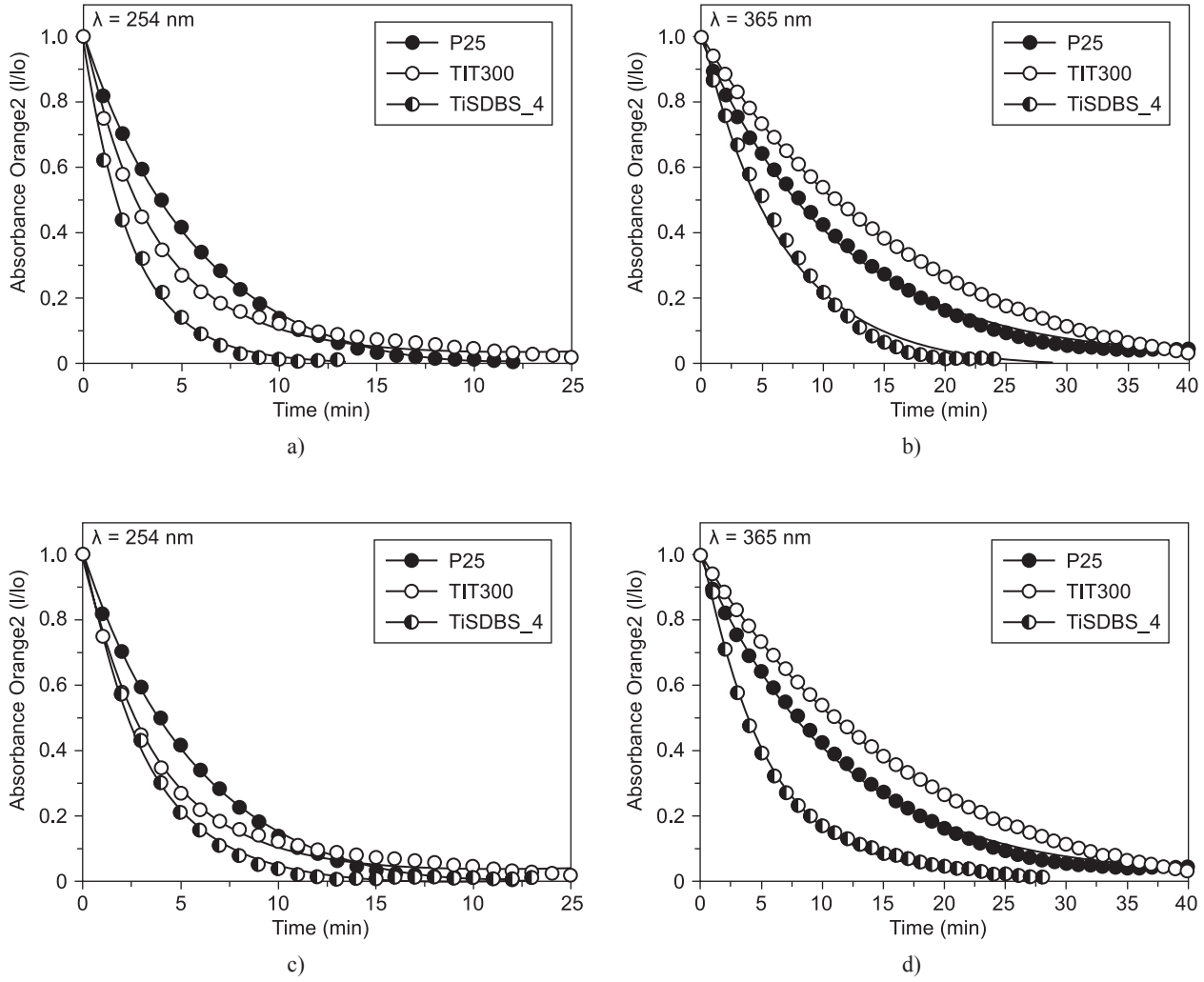

Figure 9. Photocatalytic degradation of Orange 2 dye in the presence of TiCTAB_4 and TiDCB_4 sample during irradiation at 254 nm and 365 nm wavelength.

The effect of wavelength of the UV light (germicidal white and fluorescent black lamps) on Orange 2 conversion in the photoreactor is presented in Table 2. As can be seen, the germicidal white lamp (254 nm) exhibits higher Orange 2 conversion than the fluorescent black lamp (365 nm). Germicidal white lamps are about 25 % more efficient than fluorescent black lights in producing photons with wavelengths under 385 nm [37]. In addition, it has been reported that shorter wavelength light is adsorbed more strongly by TiO_2. The electrons and holes are formed closer to the surface of the particles. Therefore, they take less time to migrate onto the surface of the particle and hence have less time to participate in energy wasting recombination reactions before useful surface (or near-surface) chemical reactions take place [38]. As a rule, in laboratory conditions, the photocatalytic properties are measured at 365nm, but for industrial purposes the use of 254 nm radiation is more effective.

CONCLUSION

Mesoporous titania was prepared by homogeneous hydrolysis of $TiOSO_4$ in aqueous solution with urea in the presence of the cationic and anionic surfactants, CTAB and SDBS, respectively. After annealing at 600°C, only pure anatase phase occurred. The resulting mesoporous samples of titania demonstrated higher photocatalytic activity compared to reference samples prepared without surfactants and to the commercial available photocatalyst Degussa P25. The application of surfactants causes changes in particle structure and properties, such as decreasing of particle size and increasing of specific surface area, which positively affect the photocatalytic activity of prepared samples. To the contrary, too high content of surfactants causes occurrence of amorphous domains and therefore decreasing of photocatalytic activity.

Acknowledgements

This work was supported by the Academy of Sciences of the Czech Republic (Project No. AV OZ 40320502) and Czech Science Foundation (Project No. 203/08/0335)

References

1. Tian C., Zhang Z., Hou J., Luo N.: Mater. Lett. *62*, 77 (2008).
2. Shibata H., Mihara H., Mukai T., Obuta T., Kohno H., Ohkubo T., Sakai H., Abe M.: Chem. Mater. *18*, 2256 (2006).
3. Cassiers K., Linssen T., Mathieu M., Bai Y.Q., Zhu H.Y., Cool P., Vansant E.F.: J. Phys. Chem. B *108*, 3713 (2004).
4. Peng T., Zhao D., Dai K., Shi W., Hirao K.: J. Phys. Chem. B *109*, 4947 (2005).
5. Wang Y., Tang X., Yin L., Huang W., Hacohen Y.R., Gedanken A.: Adv. Mater. *12*, 1183 (2000).
6. Luca V., Watson J.N., Ruschena M., Knott R. B., Chem. Mater.*18*, 1156 (2006).
7. Mohamed M.M., Bayoumy W.A., Khairy M., Mousa M.A.: Microp. Mesop. Mater. *103*, 174 (20 07).
8. Cappelletti G., Bianchi C.L., Ardizzone S.: Appl. Surf. Sci. *253*, 519 (2006).
9. Kan C., Liu X., Wang X., Ji H., Yang X., Lu L.: Colloids Surf. A: Physicochem. Eng. Aspects *311*, 93 (2007)
10. Kan C., Liu X., Duan G., Wang X., Yang X., Lu L.: J. Colloid Interface Sci. *310*, 643 (2007).
11. Sheng Q., Yuan S., Zhang J., Chen F., Microp. Mesop. Mater. *87*, 177 (2006).
12. Ren T., Yuan Z., Su B.: Chem. Phys. Lett. *374*, 170 (2003).
13. Khalil K. M.S., Zaki M. I., Powder Technology *120*, 256 (2001).
14. Jia X., He W., Luo S., Feng Y., Xu G., Li H., Zhang X.: Materials Letters *60*, 1839 (2006).
15. Sreethawong T., Suzuki Y., Yoshikawa S.: Journal of Solid State Chemistry *178*, 329 (2005).
16. Fuchs V. M., Soto E. L., Blanco M. N., Pizzio L. R.: Journal of Colloid and Interface Science *327*, 403 (2008).
17. Carbajo M. C., Enciso E., Torralvo M. J.: Colloids and Surfaces A: Physicochem. Eng. Aspects 293, 72 (2007).
18. Guo S., Wu Z., Wang H., Dong F.: Catalysis Communications *10*, 1766 (2009).
19. Gabashvili A., Major D.T., Perkas N., Gedanken A.: Ultrasonics Sonochemistry *17*, 605 (2010).
20. Jitputti J., Pavasupree S., Suzuki Y., Yoshikawa S.: Journal of Solid State Chemistry *180*, 1743 (2007).
21. Yu J., Su Y., Cheng B., Zhou M.: Journal of Molecular Catalysis A: Chemical *258*, 104 (2006).
22. Kolenko Y.V., Maximov V.D., Garshev A.V., Meskin P.E., Oleynikov N.N., Churagulov B.R.: Chemical Physics Letters *388*, 411 (2004).
23. Tian C.X.: Materials Chemistry and Physics *112*, 938 (2008).
24. Brunauer S., Emmett P.H., Teller E.: J. Am. Chem. Soc. *60*, 309 (1938).
25. Barret E.P., Joyner L.G., Halenda P.P.: J. Am. Chem. Soc. *73*, 373 (1951).
26. JCPDS PDF-2 release 2001, ICDD Newtown Square, PA, USA.
27. Scherrer P.: Göttinger Nachrichten *2*, 98 (1918).
28. Lachheb H., Puzenat E., Houas A., Ksibi M., Elaloui E., Guillard C., Herrmann J.: Appl. Catal. B: Environ. *39*, 75 (2002).
29. Štengl V., Houšková V., Bakardjieva S., Murafa N., Havlín V.: J. Phys. Chem. C *112*, 19979 (2008).
30. Monteagudo J.M., Durán A.: Chemosph. *65*, 1242 (2006).
31. Soler-Illia G., Jobbagy M., Candal R.J., Regazzoni A.E., Blesa M.A.: J. Dispers. Sci. Technol. *19*, 207 (1998).
32. Štengl V., Šubrt J., Bezdička P., Maříková M., Bakardjieva S.: Solid State Phenom. *90-91*, 121 (2003).
33. Bakardjieva S., Šubrt J., Štengl V., Dianez M.J., Sayagues M.J.: Appl. Catal. B: Environ. *58*, 193 (2005).
34. Lowell S., Shields J.E.: *Powder Surface Area and Porosity*, Chapman&Hall, London 1998.
35. Li H., Tripp C.P.: J. Phys. Chem. B *108*, 18318 (2004).
36. Macounova K., Krysova H., Ludvík J., Jirkovsky J.: J. Photochem. Photobiol. A: Chem *156*, 273 (2003).
37. Ku Y., Ma C.M., Shen Y.S.: Appl. Catal. B: Environ. *34*, 181 (2001).
38. Lim T.H., Jeong S.M., Kim S.D., Gyenis J.: J. Photochem. Photobiol. A: Chem. *134*, 209 (2000).